PAPER

Bayesian reasoning machine on a magnetotunneling junction network

To cite this article: Shamma Nasrin et al 2020 Nanotechnology 31 484001

View the <u>article online</u> for updates and enhancements.

Recent citations

- <u>Nanomagnetic Boolean Logic—The</u> <u>Tempered (and Realistic) Vision</u> Supriyo Bandyopadhyay



IOP Publishing Nanotechnology

Nanotechnology 31 (2020) 484001 (8pp)

https://doi.org/10.1088/1361-6528/abae97

Bayesian reasoning machine on a magneto-tunneling junction network

Shamma Nasrin, Justine Drobitch, Priyesh Shukla, Theja Tulabandhula, Supriyo Bandyopadhyay, and Amit Ranjan Trivedi

E-mail: snasri2@uic.edu

Received 9 March 2020, revised 14 May 2020 Accepted for publication 12 August 2020 Published 14 September 2020



Abstract

The recent trend in adapting ultra-energy-efficient (but error-prone) nanomagnetic devices to non-Boolean computing and information processing (e.g. stochastic/probabilistic computing, neuromorphic, belief networks, etc) has resulted in rapid strides in new computing modalities. Of particular interest are Bayesian networks (BN) which may see revolutionary advances when adapted to a specific type of nanomagnetic devices. Here, we develop a novel nanomagnet-based computing substrate for BN that allows high-speed sampling from an arbitrary Bayesian graph. We show that magneto-tunneling junctions (MTJs) can be used for electrically programmable 'sub-nanosecond' probability sample generation by co-optimizing voltage-controlled magnetic anisotropy and spin transfer torque. We also discuss that just by engineering local magnetostriction in the soft layers of MTJs, one can stochastically couple them for programmable conditional sample generation as well. This obviates the need for extensive energy-inefficient hardware like OP-AMPS, gates, shift-registers, etc to generate the correlations. Based on the above findings, we present an architectural design and computation flow of the MTJ network to map an arbitrary Bayesian graph where we develop circuits to program and induce switching and interactions among MTJs. Our discussed framework can lead to a new generation of stochastic computing hardware for various other computing models, such as stochastic programming and Bayesian deep learning. This can spawn a novel genre of ultra-energy-efficient, extremely powerful computing paradigms, which is a transformational advance.

Keywords: magneto-tunneling junction, Bayesian network, stochastic computing

(Some figures may appear in colour only in the online journal)

1. Introduction

Bayesian networks (BN) enable reasoning under uncertainty. Due to probabilistic graph-based learning, in BNs, inference and learning can be treated together, supervised and unsupervised learning can be merged, and missing data can be handled easily. Not surprisingly, therefore, BNs are becoming an integral component of various internet-of-things (IoT) and cyberphysical systems (CPS) [1–4].

The computation of posterior and marginal probabilities is at the cornerstone of any BN. The exact computation of these probabilities is known to be intractable for a general BN [5]. Therefore, approximate inference methods, especially stochastic simulation-based methods, are prevalent.

In stochastic simulation methods, samples of random variables in a BN are drawn to determine the posterior probabilities. To speed-up, the stochastic simulations, a variety of algorithms (survey article: [6]) explore higher sample-efficiency in Bayesian graphs. These algorithms speed-up the inference in BNs but can still fall short of the escalating pace and scale of BN-based decision engines in many IoT and CPS [7–9].

Predictions from BNs can be accelerated by a computing substrate that allows high-speed sampling from a Bayesian graph. This work discusses the development of such a platform. For the platform, mere stochasticity in devices is not enough; for scalable BNs, we need 'electrically programmable' stochasticity (to encode arbitrary probability functions,

P(x); x=0 or 1) as well as the mechanisms for stochastic interaction among devices for conditional probability, P(x|y). In this work, we show that a network of magneto-tunneling junctions (MTJs) can be used for the 'sub-nanosecond' probability sample generation. We also discuss that by exploiting magnetostriction, MTJs can also be stochastically coupled for conditional sample generation. Our discussed network also allows flexible programming of self and conditional probability parameters.

2. Background on Bayesian networks

BNs can reduce complex reasoning problems to a probabilistic graph where prior knowledge and probability theory can be used for efficient reasoning and decision-making under uncertainties. Figure 1 shows a motivating example. Using such probabilistic graphs, one can answer questions such as 'what is the likelihood of lung cancer if one visits Asia,' or 'if dyspnea occurs what are the chances that the patient is a smoker?' In IoT and CPS, such BN-based reasoning is even more versatile, and applications such as predictive maintenance [10–12], event prediction [13, 14], packet sharing in cloudedge transmission [15], anomaly detection [16–18], and sensor data fusion [19, 20] have been explored. Many of these applications operate in the real-time.

To speed up inference from stochastic simulation-based predictions, a variety of methods have been explored. In the first category, independent sampling methods such as logic sampling, likelihood sampling, and importance sampling have been developed. Sampling in these methods proceeds in the topological order, i.e. the parent nodes are sampled before the children. Independent sampling methods are, however, inefficient when dealing with the evidence on a child node. In the second category, simulation algorithms based on the Markov chain are used. The Markov chain sampling methods adjust conditional probabilities at the edges based on the evidence and sample in such a manner that the ergodicity of the Bayesian graph over sampling iterations is retained.

3. Magneto-tunneling junction-based Bayesian network nodes: MTJs with voltage-controlled probability generation

As apparent in the graph in figure 1, a BN is comprised of probabilistic nodes. In this section we discuss a novel adaptation of magnetic tunneling junction that can represent BN nodes by generating probabilistic samples where the probability of samples is programmable.

Figure 2(a) shows a p-MTJ stack with elliptical cross-section fabricated on a poled piezoelectric thin film with a soft layer in contact with the film. Both the soft and hard layers have perpendicular magnetic anisotropy. A voltage V_{VCMA} is applied across the MTJ, and at the same time, another voltage V_{St} is applied over the piezoelectric film via electrodes on the surface. The latter generates compressive strain along the major axis and tensile strain along the minor axis of the ellipse,

or vice versa, depending on the voltage polarity. The soft layer is magnetostrictive (i.e. made of a material like Co, Terfenol-D, or FeGa). The strain acts as an effective in-plane magnetic field within the soft layer around which the magnetization of the soft layer precesses when the VCMA voltage dislodges the magnetization from its initial orientation. By timing the V_{St} pulse to one-half of the precessional period, one can make the magnetization flip [22]. This flipping changes the resistance of the MTJ (low resistance when the magnetizations of the hard and soft layer are parallel and high resistance when they are antiparallel).

It is also possible to implement a controlled probability generator using an MTJ that has in-plane magnetic anisotropy instead of perpendicular magnetic anisotropy. The operating principle is the same in both cases. The perpendicular anisotropy however allows one to reduce the device footprint and makes the MTJ operation relatively tolerant of variations in the lateral dimensions.

In the presence of thermal noise at room temperature, the 'flipping' is stochastic, i.e. the magnetization will precess when V_{VCMA} is turned on and can either return back to the original orientation or flip to the other orientation. We can control the probability of flipping by adjusting the magnitude of V_{VCMA} . Therefore, the voltage V_{VCMA} provides the 'handle' to control the probability of getting either '0' or '1'.

Figure 2(b,c) show the temporal evolution of the soft layer's magnetization in the MTJ at two different V_{VCMA} considering 0.5 ns pulse duration of the voltage. We assumed elliptical soft and hard-layers with dimensions 60 nm major axis, 55 nm minor axis, and thickness 0.8 nm. The spacer layer of the MTJ was assumed to be 1.4 nm thick. The time evolution of the magnetization vector is tracked in the presence of thermal noise using the stochastic Landau–Lifshitz- Gilbert (LLG) simulations. A random white noise (magnetic) field is also included in the LLG simulations. In figure 2(d), ten thousand switching trajectories are generated, and the switching probability is the fraction of the trajectories that end up flipping. Here, the switching probability can be controlled by the voltage of V_{VCMA} .

4. Magneto-tunneling Junction-based Bayesian network edges: Magnetostrictive Interfaces for Voltage-Controlled Conditional Random Bits

In figure 1, edges are needed to conditionally couple BN nodes with another. In this section we discuss magnetostrictive interfaces for voltage-controlled correlation of MTJ-based BN nodes. MTJs are ideal for applications as computational nodes in non-Boolean paradigms, particularly in networks relying on collective models of computation where the collective activity of many elements working in concert elicit the computational activity, so the failure of a few (or sometimes even a significant fraction) of the devices does not impair the overall function. Two well-known examples of this are neuromorphic computation [23] and image processing where a few erratic pixels to not degrade the image quality appreciably. Bayesian networks fall in this category. MTJs are plagued

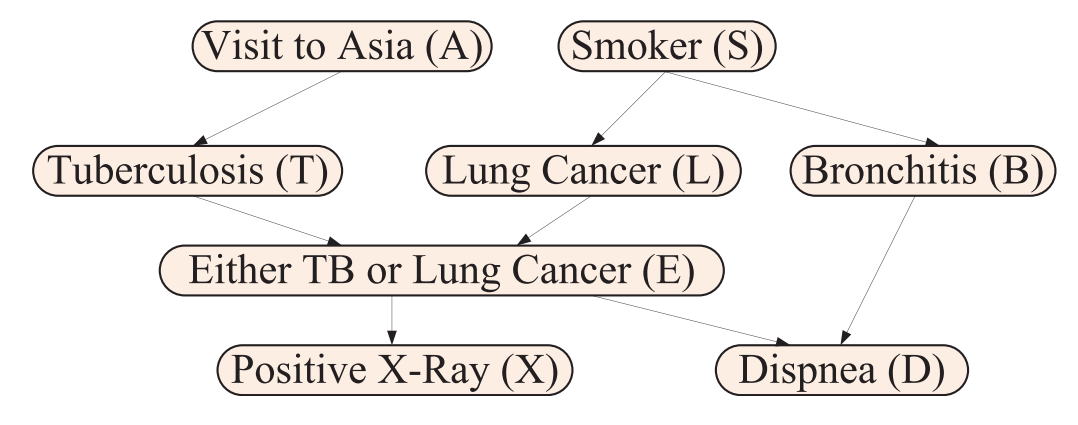


Figure 1. A motivating example of BN where probablistic relationship among variables can be encoded as a graph.

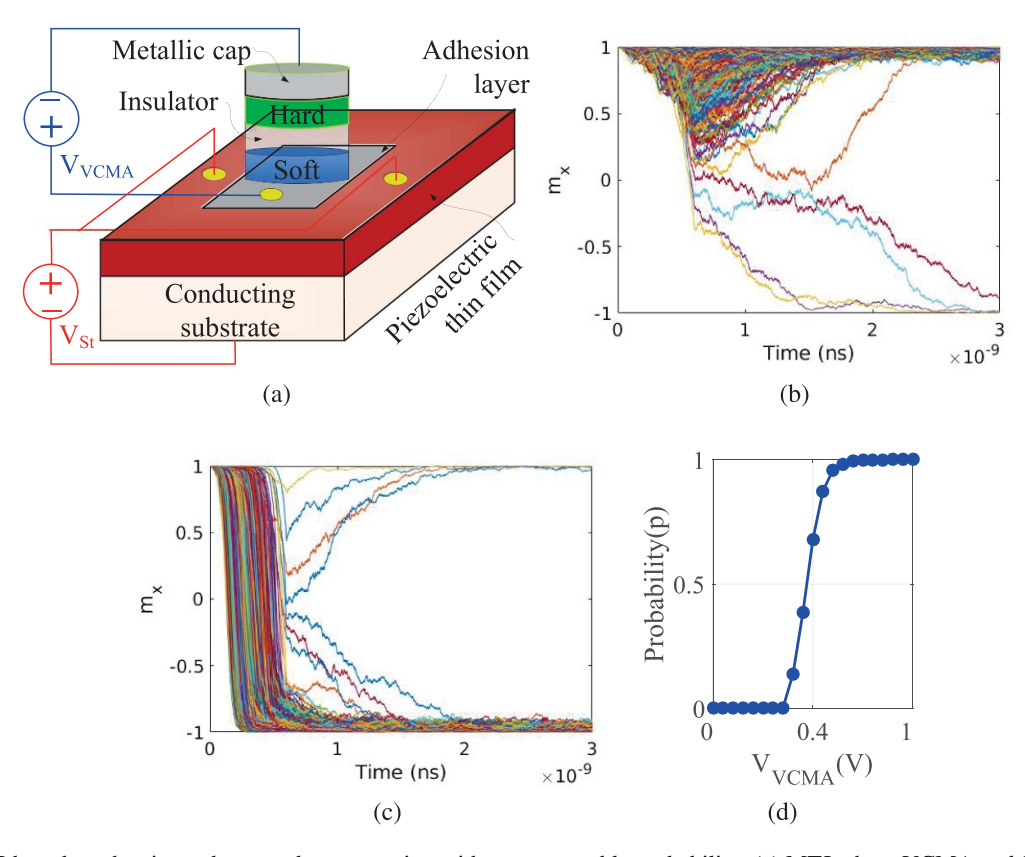


Figure 2. MTJ-based stochastic random number generation with programmable probability: (a) MTJ where VCMA and STT (applied via the voltage V_{VCMA}), and magnetostriction (strain) applied with the voltage V_{St} , can be co-optimized for programmable random number generation. Simulation results for the MTJ resistance reaching the high state for bit '0' ($m_x = +1$) and low state for bit '1' ($m_x = -1$) as a function of time for two different V_{VCMA} . (b) $V_{VCMA} = 10$ mV and (c) $V_{VCMA} = 70$ mV. (d) Switching probability characteristic with V_{VCMA} . simulations are based on the Landau–Lifshitz-Gilbert equation. © 2019 IEEE. Reprinted, with permission, from [21].

by significant device-to-device variablity and large switching error probability compared to CMOS devices, which makes them perhaps non-viable for Boolean logic that has stringent reliability requirements [24]. Non-Boolean applications are much more forgiving of variability and errors, where MTJs may find an appropriate niche. There are several recent reviews expounding the use of MTJs for computational nodes [25–28]. MTJs have also been proposed for image processing [29].

Figure 3(a) shows the integration of two MTJs to make the random bit generation in one MTJ conditionally dependent on the bit state of the other. The hard layers are composed of synthetic anti-ferromagnets that produce negligible dipole coupling field. The soft layers are composed of magnetostrictive ferromagnets. The MTJs are fabricated on a poled piezoelectric film deposited on a conducting substrate. Two electrodes are delineated on the piezoelectric film with appropriate dimensions and spacing. With an applied voltage of appropriate polarity, the electrodes generate biaxial strain underneath the magnetostrictive soft layer of MTJ-B. By varying the voltage at the electrodes, we can vary the magnitude of strain experienced by the magnetostrictive soft layer of MTJ-B. The soft layer of MTJ-A also experiences strain effect, but its magnetization will be determined by the voltage applied across it, which will override any strain effect. No voltage is applied across MTJ-B. The spacing between the MTJs is made sufficiently small to have significant dipole coupling between the two soft layers.

The random bit 'A' is generated using VCMA and STTbased operating principles discussed before. To generate the random bit 'B' that is conditionally dependent on 'A,' we rely on the dipole coupling between the soft layers of MTJ-A and MTJ-B. One would expect that dipole coupling would always make the magnetization of the soft layer of MTJ-B become antiparallel to the magnetization of the soft layer of MTJ-A, but this does not happen in practice. There is a shape anisotropy energy barrier within the soft layer of MTJ-B, which will have to be overcome by dipole coupling to make its magnetization rotate from its initial orientation to become antiparallel. If the energy barrier cannot be overcome, then bit 'B' will remain in its previous state and not be anti-correlated with bit 'A.' We elucidate this in figure 3(b). Dipole coupling makes the potential asymmetric, with a barrier between them. The asymmetry depends on the bit state of MTJ-A. For example if bit A = 1, then the minimum at $\theta = 0^0$ is higher than the minimum at $\theta = 180^{\circ}$. In this case, the magnetization of MTJ-B should prefer to orient along $\theta = 180^{\circ}$ (which is the ground state), resulting in anti-correlation between bits A and B. However, this only happens probablistically under thermal noise because of the potential barrier in figure 3(b). With stress, we can modulate/depress the barrier height and therefore control the likelihood of the magnetization of MTJ-B

We have simulated the magneto-dynamics within the soft layers of both MTJ-A and MTJ-B in the presence of thermal noise by solving coupled LLG equations in the presence of a random noise field [30]. In figure 3(c), we plot the correlation parameter as a function of the stress applied to the soft layer of

MTJ-B. The results are shown at varying separations between the soft layers of MTJ-A and MTJ-B. Note that we can vary the correlation parameter from 0 (no correlation) to -1 (perfect anti-correlation) by varying the stress applied locally to the soft layer of MTJ-B with the voltage impressed between the shorted electrodes. We can also do this for any pair of bits by additional dipole-coupled MTJs.

5. Architecture of MTJ-based Bayesian Reasoning Machine

Figure 4(a) shows our grid-based architecture of coupled MTJs for Bayesian reasoning. In the topological order execution of a Bayesian graph on the grid, the parent nodes are generated in the middle column. In the first half of the clock cycle, V_{VCMA} of the respective MTJ is generated by a PMOS passing current to non-volatile memory (NVM) (figure 4(b)). The NVM can be realized using memristors or magnetic domain-wall memories. Since the proposed MTJs are realized on the top of the piezoelectric layers, the integration complexity of memristors and MTJs is low, especially for the memristor configurations discussed in [31, 32]. Additionally, since piezoelectric materials have a high dielectric constant and low leakage, dynamic charge (analog voltage) storage by realizing capacitors on the piezoelectric layer can also be explored. In the second half of the clock cycle, the parent variables evolve self-consistently in the column based on the dipole coupling voltages.

In the successive clock cycles for the evolution of child nodes, the first half of the cycle generates the coupling voltage in the piezoelectric couplers and the second half cycle generates the child nodes. With increasing clock cycles, the sampling progresses away from the parent column and samples child nodes hierarchically down in a Bayesian graph. In figure 4(a), the potential of piezoelectric couplers can be similarly generated using NVMs or dynamic charge storage. The bias current to NVMs in a column is turned off as the sampling moves to the next column. The output of a random node can be read as in typical MTJ-based memory arrays using select transistors and row/column peripherals [33]. Note that typical BN applications read posterior probability at only a few variables. Therefore, only a few nodes in the MTJ grid need to be read after each sampling iteration, and the reading overheads are low in the MTJ grid.

5.1. Mapping general Bayesian graphs on 2D MTJ grid

Our MTJ grid only enables the nearest neighbor correlation, where each node can only have binary states. Therefore, new mapping and graph partitioning/restructuring algorithms are needed to compile a general Bayesian graph on the 2D grid. Nodes with more than two states can be split by binary coding. To execute general edges in a graph, in figure 5, an example mapping strategy is shown where graph nodes are duplicated by setting the coupling voltages for perfect anti-correlation (and swapping '1' and '0' convention at the interleaved rows). The key objectives for an optimal

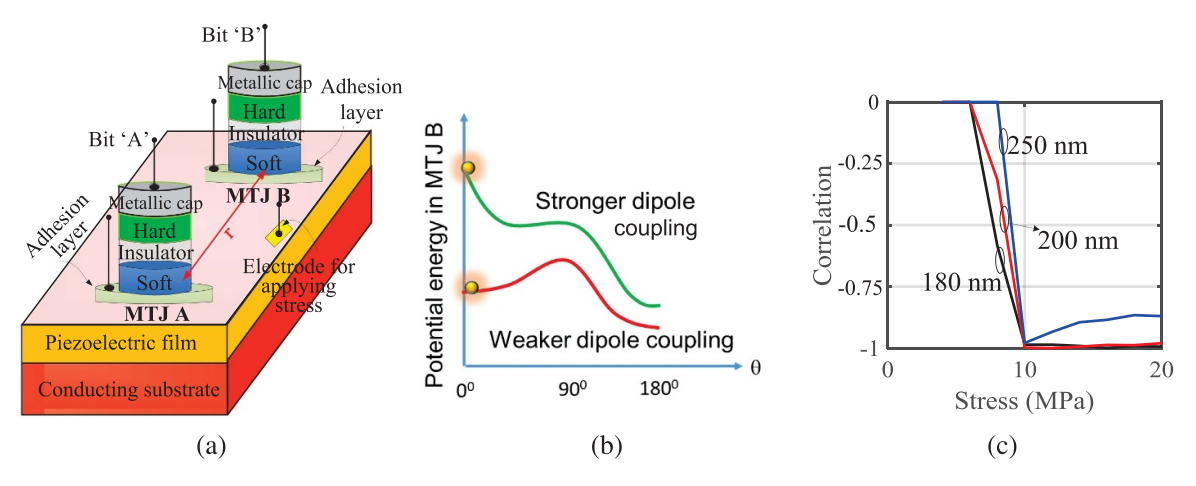


Figure 3. (a) MTJ integration where the effect of dipole coupling, controlled with local stress applied to one MTJ, can be utilized to stochastically couple the switching probability of one MTJ depending on the state of the other. This results electrically tunable correlation between the bits 'A' and 'B' encoded in the resistance states of the two MTJs. (b) Potential energy in MTJ-B as a function of its free layer magnetization orientation depicted by the angle θ . The potential energy barrier can be modulated by strain which then controls the likelihood of MTJ-B switching in response to the bit state of MTJ-A. (c) Correlation of two MTJ random bits at varying stress level. The correlation also depends on the center to center separation between MTJ disks. Reproduced with permission from [30].

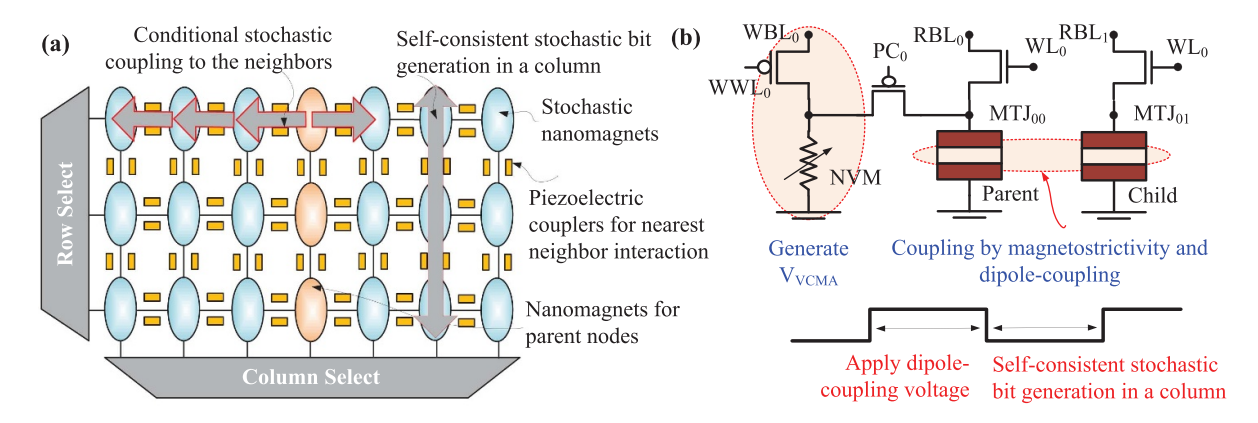


Figure 4. MTJ network-based Bayesian reasoning machine: (a) schematic of the architecture. (b) Cell schematic for parent and child nodes.

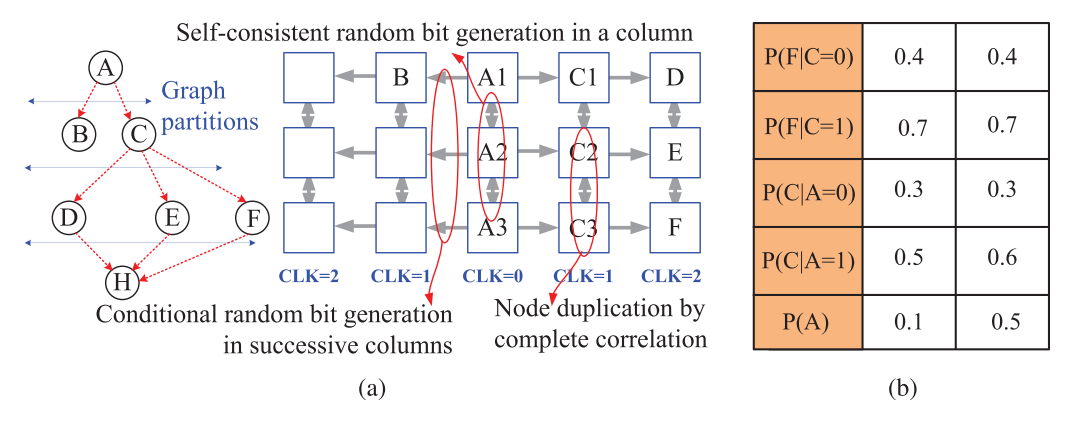


Figure 5. An example mapping of Bayesian graph on 2D nanomagnet grid.

mapping algorithm are: (i) minimize replication of graph nodes and (ii) minimize the distance of the farthest node from the central column (to maximize sampling iteration speed).

5.2. Mapping different sampling algorithms on the grid

Independent sampling can be implemented on the MTJ-grid by mapping the parent variables on the parent MTJ column

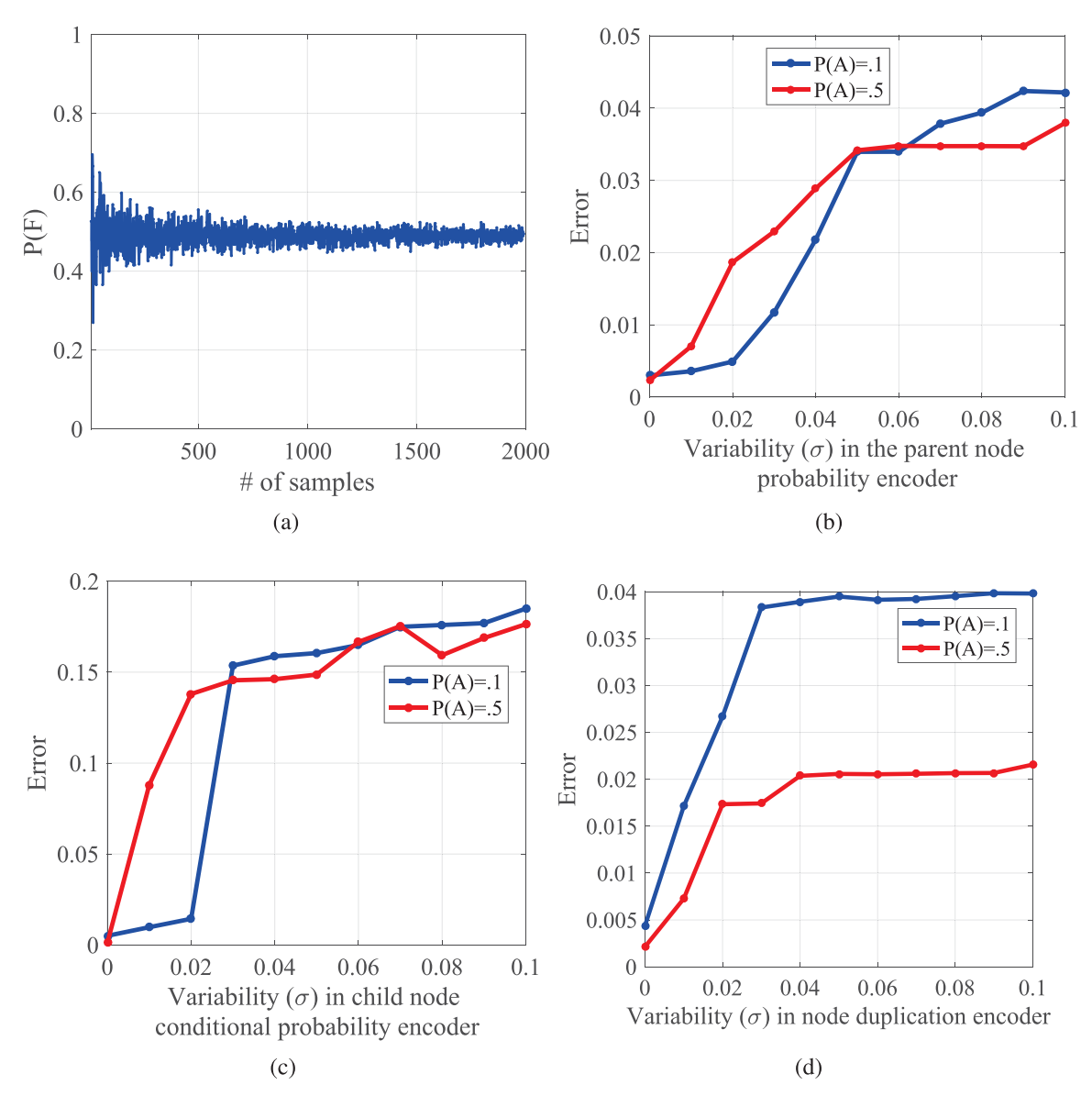


Figure 6. Different non-idealities arise in MTJ-based Bayeasian network implementation. (a) Impact of number of samples on the probability of node F. Higher number of samples results in stable probability estimation. (b) Non-ideality in the parent node A encoding causes error in the probability approximation. Here, we studied non-ideality for two different cases: P(A) = 0.5 and P(A) = 0.1. (c) Error arises from the non-ideality in child node C encoding. (d). Effect of variability in self correlation encoding on the probability approximation.

and then mapping the children on the successive columns. Rejection and likelihood sampling can be implemented by programming the read peripherals, and unlikely samples can be discarded or weighted lower. Importance sampling can be implemented by reprogramming the voltages of piezoelectric couplers to tweak the correlation parameters as sampling iterations proceed. Markov chain-based sampling algorithms update edge correlation value as the sampling chain evolves.

6. Simulation results

Considering the graph shown in figure 5 as a test-case. In this section, we study the impact of various non-idealities on inference accuracy. In figure 6 for our MTJ-based Bayesian

network implementation, the non-idealities arise due to: (1) imprecise gate-controlled probabilistic switching in the parent node MTJ, (2) imprecise dipole coupling between MTJs, and (3) imprecise non-volatile memory resistance. We consider a forward sampling flow to compute P(F) to characterize the above non-ideality sources. The designed probability parameters for the parent node and conditional dependence on child nodes are also shown in figure 5.

In figure 6(a), we show the evaluated P(F) at the increasing number of samples from the graph. Note that an adequately high sample size is needed for high confidence (low variance) prediction. Moreover, in more complex and larger graph structures, the number of samples for high confidence inference also increases dramatically. Therefore, software-based approaches do not scale for inference in complex

and larger graph structures under real-time constraints. Our approach allows sub-ns sample generation; therefore, it can operate on much larger graph structures under performance constraints.

In figure 6(b), we study the impact of variability in parent node probability encoding. In figure 4(b), the parent node probability is encoded by biasing the parent MTJ through a resistive memory and current bias. Under process imperfections, resistive memory resistance, as well as bias current, may vary; moreover, the characteristics of the parent MTJ itself can deviate. As a result, the encoded probability parameter varies under process variation. We lump different process variability sources and treat the parent node probability parameter as $\mathcal{N}(P_p, \sigma_P^2)$. Here, P_p is the programmed parent node probability, and σ_P^2 is the expected variance due to process variability sources discussed earlier. Figure 6(b) shows that with higher degree of process variability (high σ_P^2), prediction error for P(F) increases. Tolerance to process variability in our design can be increased by upsizing the components (resistive memory, current biasing transistor, etc) as well as post-fabrication calibration (which we plan to address in a future work).

In figure 6(c), we study the impact of variability in child node probability encoding. In figure 4(b), the conditional probability of child nodes is encoded by the dipole coupling of parent and child node MTJ. The dipole coupling strength is programmed by applying the potential to piezoelectric film, and thereby, by programming stress fields. Under process imperfections, the applied potential and potential-induced stress fields can vary. Similar to the parent nodes, we lump different process variability sources and treat child node probability parameter as $\mathcal{N}(P_c, \sigma_C^2)$. Here, P_c is the programmed parent node probability and σ_C^2 is the expected variance. Figure 6(c) shows that with higher degree of process variability (high σ_C^2), prediction error for P(F) increases. Therefore, effective mechanisms to contain process variability impact is necessary. Figure 6(d) shows a similar study as in figure 6(c) but for node duplication. In the considered test-case, we see a strong dependence between graph probability parameters and process variability. Notably, the case where P(A) = 0.1is a lot more sensitive to process variability than P(A) = 0.5. The result also highlights the potential to co-design graph structure and parameters considering process variability sources.

7. Conclusions

We have discussed principled approaches to co-optimize VCMA, STT, and magnetostrictivity effects in an MTJ to engineer useful stochasticity and probabilistic interaction among MTJs. Co-adapted MTJs are quite suited for subns sampling as well as encoding conditional probabilistic dependences. Based on the novel adaptation of MTJ, a variety of Bayesian inference-based algorithms can be accelerated. Specifically for Bayesian networks, we have also discussed 2D grid-based mapping strategy and peripheral circuits to map arbitrary-shaped graphs on the proposed MTJ grid. This work

has also studied the sources and impact of various process variability mechanisms on inference accuracy.

ORCID iDs

Shamma Nasrin

https://orcid.org/0000-0002-6439-768X

Justine Drobitch

https://orcid.org/0000-0002-4439-7551

Theja Tulabandhula

https://orcid.org/0000-0001-9111-7519

Supriyo Bandyopadhyay

https://orcid.org/0000-0001-6074-1212

References

- [1] Jun C and Chi C 2014 Design of complex event-processing ids in internet of things 2014 Sixth Int. Conf. on Measuring Technology and Mechatronics Automation IEEE pp 226–9
- [2] Kumar N, Rodrigues J J and Chilamkurti N 2014 Bayesian coalition game as-a-service for content distribution in internet of vehicles *IEEE Internet Things J.* 1 544–55
- [3] Siryani J, Tanju B and Eveleigh T J 2017 A machine learning decision-support system improves the internet of things' smart meter operations *IEEE Internet Things J.* 4 1056–66
- [4] Park H-S, Oh K and Cho S-B 2011 Bayesian network-based high-level context recognition for mobile context sharing in cyber-physical system *Int. J. Distributed Sensor Networks* 7 650387
- [5] Barber D 2012 Bayesian Reasoning and Machine Learning (Cambridge: Cambridge University Press)
- [6] Guo H and Hsu W 2002 A Survey of Algorithms for Real-Time Bayesian Network Inference (Join Workshop on Real Time Decision Support and Diagnosis Systems)
- [7] Louizos C, Ullrich K and Welling M 2017 Bayesian Compression for Deep Learning (Advances in Neural Information Processing Systems) pp 3288–98
- [8] Li Z, Li P, Krishnan A and Liu J 2011 Large-scale dynamic gene regulatory network inference combining differential equation models with local dynamic bayesian network analysis *Bioinformatics* 27 2686–91
- [9] Bronstein A, Das J, Duro M, Friedrich R, Kleyner G, Mueller M, Singhal S and Cohen I 2001 Self-Aware Services: Using Bayesian Networks for Detecting Anomalies in Internet-Based Services (Piscataway, NJ: IEEE) pp 623–38
- [10] Yam R, Tse P, Li L and Tu P 2001 Intelligent predictive decision support system for condition-based maintenance Int. J. Adv. Manufacturing Technol. 17 383–91
- [11] Gilabert E and Arnaiz A 2006 Intelligent automation systems for predictive maintenance: A case study *Robot*. *Comput.-Integr. Manuf.* **22** 543–9
- [12] Van Koten C and Gray A 2006 An application of bayesian network for predicting object-oriented software maintainability *Inf. Softw. Technol.* 48 59–67
- [13] Sahoo R K, Oliner A J, Rish I, Gupta M, Moreira J E, Ma S, Vilalta R and Sivasubramaniam A 2003 Critical event prediction for proactive management in large-scale computer clusters *Proc. of the Ninth ACM SIGKDD International Conference on Knowledge Discovery and Data Mining* ACM pp 426–35
- [14] Cheon S-P, Kim S, Lee S-Y and Lee C-B 2009 Bayesian networks based rare event prediction with sensor data *Knowl.-Based Syst.* 22 336–43
- [15] Vegni A M, Loscri V, Neri A and Leo M 2016 A bayesian packet sharing approach for noisy iot scenarios 2016 IEEE

- First Int. Conf. on Internet-of-Things Design and Implementation (IoTDI) IEEE pp 305–8
- [16] Wong W-K, Moore A W, Cooper G F and Wagner M M 2003 Bayesian network anomaly pattern detection for disease outbreaks *Proc. of the 20th Int. Conf. on Machine Learning* (ICML-03) pp 808–15
- [17] Kruegel C, Mutz D, Robertson W and Valeur F 2003 Bayesian event classification for intrusion detection 19th Annual Computer Security Conf. 2003 Proc. IEEE pp 14–23
- [18] Heard N A, Weston D J, Platanioti K and Hand D J 2010 Bayesian anomaly detection methods for social networks Annals Appl. Stat. 4 645–62
- [19] Guerriero M, Svensson L and Willett P 2010 Bayesian data fusion for distributed target detection in sensor networks IEEE Trans. Signal Process. 58 3417–21
- [20] Zhang Y and Ji Q 2006 Active and dynamic information fusion for multisensor systems with dynamic bayesian networks *IEEE Trans. Syst. Man Cybernetics* B 36 467–72
- [21] Nasrin S, Drobitch J L, Bandyopadhyay S and Trivedi A R 2019 Mixed-mode magnetic tunnel junction-based deep belief network 2019 IEEE 19th Int. Conf. on Nanotechnology (IEEE-NANO) IEEE pp 443–8
- [22] Drobitch J L, Abeed M A and Bandyopadhyay S 2017 Precessional switching of a perpendicular anisotropy magneto-tunneling junction without a magnetic field *Japan. J. Appl. Phys.* 56 100309
- [23] Roychowdhury V P, Janes D B, Bandyopadhyay S and Wang X D 1996 Collective computational activity in self-assembled arrays of quantum dots: A novel neuromorphic architecture for nanoelectronics *IEEE Trans*. *Electron Devices* 43 1688–99
- [24] Winters D, Abeed M A, Sourav S, Barman A and Bandyopadhyay S 2019 Reliability of magnetoelastic

- switching of non-ideal nanomagnets with defects: A case study for the viability of straintronic logic and memory *Phys. Rev. Appl.* **12** 034010
- [25] Sengupta A and Roy K 2017 Encoding neural and synaptic functionalities in electron spin: A pathway to efficient neuromorphic computing Appl. Phys. Rev. 4 041105
- [26] Grollier J, Querlioz D and Stiles M D 2016 Spintronic nanodevices for bio-inspired computing *Proc. IEEE* 104 2024
- [27] Camsari K Y, Debashis P, Ostwal V, Pervaiz A Z, Shen T, Chen Z, Datta S and Appenzeller J 2020 From charge to spin and spin to charge: Stochastic magnets for probabilistic switching *Proc. of the IEEE* pp 1–16
- [28] D'Souza N et al 2018 Energy-efficient switching of nanomagnets for computing: straintronics and other methodologies Nanotechnology 29 442001 aug
- [29] Abeed M A, Biswas A K, Mamun A-R M, Atulasimha J and Bandyopadhyay S 2017 Image processing with dipole-coupled nanomagnets: Noise suppression and edge enhancement detection *IEEE Trans. Electron Devices* 64 2417–24
- [30] McCray M, Abeed M A and Bandyopadhyay S 2019 A nanomagnetic voltage-tunable correlation generator between two random bit streams for stochastic computing arXiv:1907.07532
- [31] Sangwan V K, Lee H-S, Bergeron H, Balla I, Beck M E, Chen K-S and Hersam M C 2018 Multi-terminal memtransistors from polycrystalline monolayer molybdenum disulfide *Nature* 554 500
- [32] Xia Q et al 2009 Memristor- cmos hybrid integrated circuits for reconfigurable logic Nano Lett. 9 3640–5
- [33] Wang K, Alzate J and Amiri P K 2013 Low-power non-volatile spintronic memory: Stt-ram and beyond J. Phys. D: Appl. Phys. 46 074003